VIBRATIONAL CHARACTERISTICS OF BRAIN MAGNETIC RESONANCE ELASTOGRAPHY

BY

CURTIS LAURENCE JOHNSON

THESIS

Submitted in partial fulfillment of the requirements
for the degree of Master of Science in Mechanical Engineering
in the Graduate College of the
University of Illinois at Urbana-Champaign, 2010

Urbana, Illinois

Adviser:

Professor John G. Georgiadis

Abstract

This thesis aims to investigate vibrational characteristics of magnetic resonance elastography (MRE) of the brain. MRE is a promising, non-invasive methodology for the mapping of shear stiffness of the brain. A mechanical actuator shakes the brain and generates shear waves, which are then imaged with a special MRI sequence sensitive to sub-millimeter displacements. This research focuses on exploring the profile of vibrations utilized in brain elastography from the standpoint of ultimately investigating nonlinear behavior of the tissue. The first objective seeks to demonstrate the effects of encoding off-frequency vibrations using standard MRE methodologies. Vibrations of this nature can arise from nonlinearities in the system and contaminate the results of the measurement. The second objective is to probe nonlinearity in the dynamic brain system using MRE. A non-parametric decomposition technique, novel to the MRE field, is introduced and investigated.

Acknowledgments

I appreciate the many people who supported me during my time at the University of Illinois. Many thanks to my adviser, Dr. John G. Georgiadis, who saw my enthusiasm and willingness to work and gave me the opportunities to make this work happen. I also want to thank all of my group members for their guidance and special thanks to Dr. Dimitrios C. Karampinos and Mr. Danchin Chen for their continued help despite all the long scan sessions, and Mr. Max Snow and Mr. Eeshan Kumar for their assistance in the lab. I am grateful to all my friends for their support and contributions to my work. Finally, thanks to my family for all their love and for support during my studies and through my life.

Table of Contents

List of Tables

List of Figures

Chapter 1

Introduction

1.1 Magnetic Resonance Elastography

The use of mechanical properties of biologic tissue as biomarkers for disease and pathology has a long history. For example, the first step in detection of a breast lesion or liver fibrosis is often manual palpation of the tissue, which can be followed by imaging and biopsy. Palpation provides a qualitative assessment of the stiffness of the tissue, but quantitative stiffness measures could allow for improved detection of pathology, and could also provide information regarding the staging of the disease. Additionally, palpation is not an option for tissues that are protected by bony structures, such as the brain or heart.

Magnetic resonance elastography (MRE) is an emerging technique for quantitatively probing the mechanical properties of tissue non-invasively [1, 2]. MRE utilizes magnetic resonance imaging (MRI) to capture displacement and deformation of materials being imaged. The displacement is generated externally through periodic mechanical actuation, which induces shear waves in the tissue of interest. Snapshots of the local displacements associated with the shear wave motion are obtained by synchronizing the MRI acquisition. The shear wave patterns are the inputs to a wave inversion technique to extract the elastic properties of the material [3]. MRE methods have been used to investigate the stiffness of a variety of tissues in vivo including liver [4, 5, 6], breast [7, 8, 9], skeletal muscle [10, 11, 12, 13], heart [14, 15], and brain [16, 17, 18, 19, 20, 21, 22].

The work presented in this thesis focuses on brain, and the specific challenges the MRE investigator faces when examining the tissue. The human brain is a complex organ with tissue which exhibits complex physiological and mechanical properties. Our scope here is limited to the passive mechanical properties of brain tissue. The dynamic brain system, comprising the cranium, blood, cerebrospinal fluid, and brain parenchyma, may exhibit nonlinearities in dynamic response [23, 24, 25, 26]. These nonlinearities unquestionably introduce poor repeatability and reproducibility of MRE results in the brain. As is the case with engineered systems, these problems are caused by incomplete definition of the dynamic system and its

constraints.

MRE techniques are in an infantile state relative to similar methods for nondestructive evaluation of engineered materials. Much of the MRE literature refers to wave motion and propagation, which indicate transient phenomena, whereas the displacements measured are technically vibrations because the phenomenon has achieved steady-state. Further, the described wave propagation, governed by the imaginary part of the signal, actually provides evidence of complex modes of vibration. Complex modes themselves are an indication of non-proportional damping in the material [27], a consequence of the viscoelastic nature of biologic tissues.

Modes of vibration are intrinsic characteristics of dynamic systems arising from system parameters such as stiffness and damping [28], which are of interest in MRE experiments. The dynamic response of a system is a combination of all the excited modes, which are determined by the type of external forcing [29]. In the case of traditional MRE, the forcing used has a constant amplitude and a single frequency. For linear systems, the response to periodic forcing is at the same frequency, with the excited mode depending on that frequency. When the system is nonlinear, the excited mode is still governed by the external forcing, though determining the specific response is more complicated. The frequency of the forcing still has a significant impact, yet the dynamic response will depend on whether the system is stable at its equilibrium points. The dynamic response is further governed by frequency-amplitude relationships near these points, and is highly dependent on amplitude of forcing and other initial conditions. The dependence on specific properties of the system as well as parameters of the forcing can be modeled by employing bifurcation theory [30].

The methodologies of clinical MRE have been based on linear, or linearized, dynamics of the system and have largely ignored the deleterious effects of nonlinearities corrupting the assumed linear response. This work aims to serve as the basis for future nonlinear investigations of clinical MRE so as to further the methodology and improve the reliability of the results.

1.1.1 Objectives

The following chapters seek to demonstrate and study how incorrect assumptions regarding the brain can confound standard MRE results, with the aim of informing the future advances in the field of brain MRE.

In chapter two, we investigated the effects of conducting MRE experiments with inappropriate assumptions regarding the mechanical excitation and specifically the frequency of vibration. Current methods in MRE rely on the harmonic nature of the displacement to simplify the wave inversion process, but also in designing the data acquisition scheme. The aim of this chapter is to elucidate errors in shear

stiffness estimates when MRE experiments are performed assuming an incorrect frequency of vibration, a possible scenario when considering the complexities of the dynamic brain system.

Classical MRE methods utilize the Fourier transform to calculate wave displacement patterns given a set of rigid assumptions. In chapter three, we demonstrate an improved data processing method to extract vibration modes from wave images in brain MRE. The aim is to investigate how nonlinearities in the system can lead to irreproducible results, and to outline the use of an alternative methodology in the form of the proper orthogonal decomposition.

1.2 MRE Methodology

1.2.1 MRE Hardware

One of the most important considerations in MRE is how shear waves are generated in the tissue of interest [31, 32]. In order to be compatible with MRI, a certain number of limitations are introduced in the mechanical actuation system. Specifically, the system must not be composed of metal parts unless properly shielded, and even then it must not cause interference with the imaging through the MRI scanner. In addition, the tissue to be actuated is located within the bore of the scanner, and thus there is very little room to place components of the actuator near the tissue itself. Due to these limitations, the majority of MRE hardware falls in to one of three categories: electromechanical [33, 34], piezoelectric [35], and pneumatic [36].

For the brain, as opposed to other tissues, shear wave generation is made difficult by the lack of ability to actuate the tissue directly. Shear waves are generated through inertial forces by vibrating the subject's cranium, and significant forces are required to obtain the necessary displacements transmitted to the brain tissue itself. To this end, most published brain MRE work use electromechanical actuation systems in either local [16, 18] or remote configurations [17, 37].

Local configurations consist of a device attached to the inside of the head coil in the MRI scanner and actuation is performed by utilizing the static B_0 magnetic field of the scanner. Controlled electrical current is pulsed through the actuator to generate displacement. A bite bar is driven by the actuator to induce motion of the subject's head in the left-right direction. The local bite bar configuration provides improved control of the imposed motion due to improved coupling of the system, but it is a more complicated system that is known to be uncomfortable for subjects [16, 20].

The remote configuration involves an electromechanical shaker and amplifier system which are located far from the scanner and placed in a Faraday cage as to allow for the inclusion of active, metal components

while maintaining safety and removing interference in the imaging. The shaker is attached to a head rocker that is attached inside the head coil through by means of a long rod, as shown in Figure 1.1(a). The subject's head rests on the rocker, as shown in Figure 1.1(b), and the remote shaker provides motion in the "nodding" direction. This remote configuration is convenient, flexible, and can be modified more easily than the local configurations. The remote configuration has been used in the majority of previous studies, and is employed in this work.

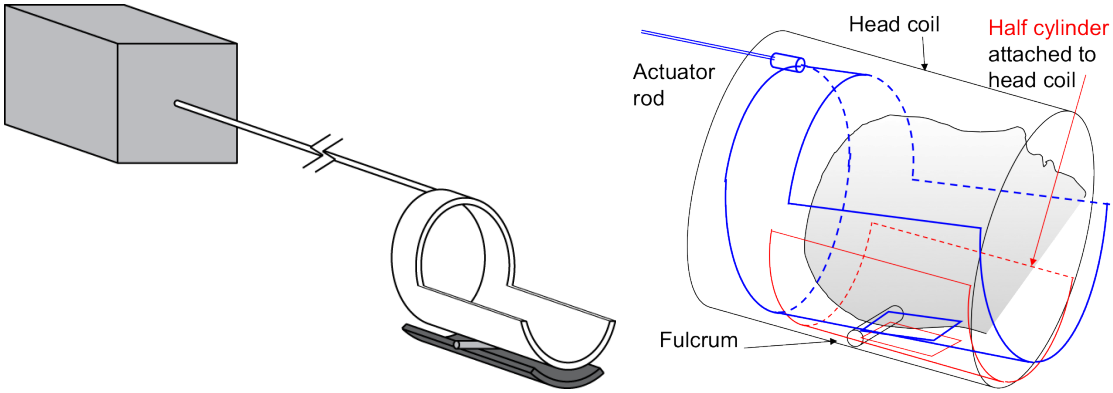

Figure 1.1: (a) Shaker, rod, and rocker system used for brain MRE; (b) detail of rocker with subject's head

1.2.2 MRE Imaging

MRE is a phase-contrast MRI technique that incorporates motion-encoding gradients in to standard MRI sequences in order to map displacement through phase. In the presence of magnetic field gradients, any displacement of spins in the direction of the gradients causes the spins to accumulate phase [1]. The amount of phase acquired depends on the integral of displacement in time and the strength of the gradient field. By controlling the period of the motion and the applied gradients, the amount of actual displacement can be back calculated from the phase map.

In the classic dynamic MRE experiment, shear waves are generated through harmonic actuation at a known frequency, typically in the acoustic range of 50-200 Hz [3]. By applying bipolar gradients with the same frequency and period of motion, MRE is capable of capturing the displacement at the same frequency, while maximizing contrast and maintaining gradient balance. By locking the period of the gradients with the period of the motion, the following expression can be derived for the accumulated phase, ϕ, in terms of displacement (Eq. 1.1):

$$\phi\left(r\right) = \frac{2\gamma \cdot \tau \cdot G \cdot u_0 cos\left(r\right)}{\pi} sin\left(k \cdot r\right), \tag{1.1}$$

where γ is the gyromagnetic ratio of the spins, τ is the period of motion, G is the gradient strength, and u_0 is the displacement amplitude. The phase is a function of both spatial position, r, and wave number, k.

In typical MRE experiments, the procedure for acquiring a single wave image is repeated in time to investigate wave propagation through space [38]. By synchronizing the imaging sequence to the motion generation, the phase of the imaged wave can be controlled by manipulating a small delay. The delay, Δt, causes a phase offset in the motion, θ, based on the vibration period, and the resulting MRI phase from Eq. 1.1 is now given by Eq. 1.2 [1]:

$$\phi\left(r,\theta\right)=\frac{2\gamma\cdot\tau\cdot G\cdot u_0 cos\left(r\right)}{\pi}sin\left(k\cdot r+\theta\right), \tag{1.2}$$

The imposed phase offsets generally span a single period of actuation, and the resulting time series of displacements at each voxel are Fourier transformed to isolate the harmonic of interest [3, 7]. This processing step serves to provide information about complex wave propagation, but also as a de-noising technique to remove higher harmonics [39].

Virtually any MRI sequence can be modified to include the gradients necessary for MRE experiments [40, 41, 42, 43, 44, 45]. The major considerations for designing a sequence are speed, resolution, contrast, and tissue type. Speed is the most important of considerations as it directly relates to patient comfort. Since the tissue of interest is mechanically shaken for nearly the entire scan time, minimizing the required scanning time is of utmost importance. Maximizing speed comes at the cost of resolution, which has different requirements for different tissues depending on the spatial order of magnitude of the features of interest. Some sequences, such as balanced steady-state free precession, have very complicated phase models, making their application to MRE very difficult. Other sequences, such as echo-planar imaging, have poor responses to fat content in the tissue, thus limiting usefulness in fatty tissue, such as the breast.

For brain MRE, the comfort of the subject is critical, since the brain is more sensitive to mechanical actuation than other organs. To address this issue, this work uses an EPI-MRE sequence, a diagram of which is shown in Figure 1.2. Due to the low fat content of brain tissue this is an acceptable sequence, and also allows for a short scan time of approximately one minute. EPI does have a relatively low spatial resolution, obscuring some of the finer spatial features in the brain, but it allows for a higher temporal resolution in order to investigate the vibrational response of the system.

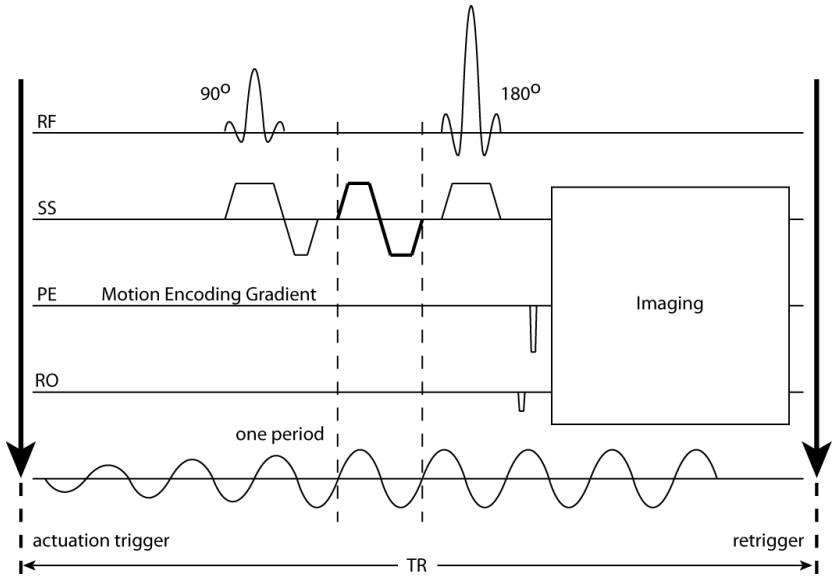

Figure 1.2: Modified EPI sequence for MRE

1.2.3 MRE Inversion

The final step in MRE techniques is to determine the mechanical properties of material from the wave image. This requires the inversion of the appropriate wave equation governing the material. In general, all materials in MRE experiments are assumed to be linear, homogeneous, and isotropic in order to simplify the inversion process [3, 46], though some work has been done to incorporate more complex material models into inversion schemes [12, 47, 48, 49].

The wave equation governing the displacements in MRE is derived from the elastic material constitutive law (Eq. 1.3):

$$\rho \frac{\partial^2 u_i}{\partial t^2} = \mu \frac{\partial^2 u_i}{\partial x_j^2} + (\mu + \lambda) \frac{\partial^2 u_j}{\partial x_i \partial x_j}, \tag{1.3}$$

where λ is the first Lamé coefficient and μ is the second, also known as the shear modulus. Fluid-filled biological materials are nearly incompressible, which simplifies the elastic wave equation to the Helmholtz Equation (Eq. 1.4):

$$\rho \frac{\partial^2 u_i}{\partial t^2} = \mu \frac{\partial^2 u_i}{\partial x_j^2}. \tag{1.4}$$

By further recognizing that the motion, u, is harmonic at the imposed frequency, ω, we can express it as (Eq. 1.5)

$$u_i(t) = u_i cos(\omega t), \tag{1.5}$$

and the time dependence of the Helmholtz Equation cancels, further simplifying it to (Eq. 1.6):

$$-\rho\omega^2 u_i = \mu \frac{\partial^2 u_i}{\partial x_j^2}. \tag{1.6}$$

This equation directly relates the measured displacement to the shear modulus by means of the driving frequency and material density.

There are two major techniques for inverting the Helmholtz Equation in MRE methodology: local frequency estimation (LFE) [50, 51] and algebraic inversion of the direct equation (AIDE) [46, 52]. LFE techniques seek to derive the spatial frequency of the wave propagation and relate it to stiffness. Its applicability is found in incompressible and homogeneous materials, and has been shown to provide robust and useful estimates of shear modulus in MRE. The AIDE technique does not seek to estimate spatial frequency, but rather tries to solve the simplified wave equation directly. Direct inversion is beneficial compared to LFE by allowing for more complicated material property models, such as viscoelasticity, to be incorporated more easily, but suffers from the drawback of requiring the calculation of spatial derivatives from pointwise data. In this work, LFE inversion processes were employed [53].

Chapter 2

On the Effect of Off-Frequency Encoding in MR Elastography

2.1 Introduction

The feasibility of extracting meaningful information regarding stiffness of tissue with MRE hinges on the ability to invert the acquired image using the appropriate wave theory. In order to perform a valid inversion, a number of simplifications must be made regarding the material properties. Specifically, assumptions about the tissue's anisotropy, viscoelasticity, and linearity must all be accounted for in the wave inversion procedure. Advanced acquisition and reconstruction schemes have been used to investigate anisotropic and viscoelastic properties of tissues with MRE in order to achieve a more accurate understanding of the underlying tissue properties. Nonlinear material behavior of the tissue is expected, and has been investigated previously with MRE [54], but the assumption of linearity holds for the small displacements that are generally used.

In addition to assumptions regarding the materials being imaged, there are assumptions regarding the applied motion to the tissue. In dynamic elastography the motion is assumed to be harmonic at the controlled input driving frequency. The control of the input frequency is used to not only achieve optimal wave profiles in the tissue, but it also determines the required imaging parameters. The input frequency is typically used to determine the encoding gradient duration [41], the timing delay for phase offsets [38], and traditional imaging parameters such as the echo time (TE) and the repetition time (TR) [7]. For the actual vibration frequency to be different than the input, the dynamic system will need to be nonlinear. In many applications of MRE, the method of actuation can be assumed linear because of adequate mechanical coupling with the tissue. When actuation remote systems are used, the presence of nonlinearities is more likely, but work has been done to characterize the mechanical input spectra of such systems [55]. However, in brain MRE, the coupling between the actuator and the tissue is more complex, and the cranium, cerebrospinal fluid, and tissue geometry can account for nonlinearities in the system.

In this work we investigated the effects of performing MRE experiments with a driving frequency

assumed incorrectly. Numerical simulations, phantoms, and in vivo brain experiments were performed in order to demonstrate how stiffness estimates could be skewed on both a global and local level by tailoring an MRE experiment to the wrong frequency.

2.2 Theory

During time-harmonic elastography, the motion of mechanically actuated tissue or material is mapped by encoding the displacement of the water proton spins. The motion of each spin, u, is sinusoidal and can be described by the following function (Eq. 2.1):

$$u\left(t\right) = u_0 cos\left(\mathbf{k}\cdot\mathbf{r} + \omega t\right), \tag{2.1}$$

where u_0 is the amplitude of the spin displacement, ω is the angular frequency of the vibrations, $\mathbf{k}$ is the wave vector, and $\mathbf{r}$ the spatial position of the spin. The product of $\mathbf{k}$ and $\mathbf{r}$ describes the spatial phase of a wave at a given point. It is now useful to reformulate the displacement to include the offset phase between mechanical vibration and motion encoding, θ, as well as to amplify the effect of the vibration frequency (Eq. 2.2):

$$u\left(t\right) = u_0 cos\left(\mathbf{k}\cdot\mathbf{r} + \omega_v t + \theta\right), \tag{2.2}$$

where ω_v is the angular frequency of the oscillatory spin displacement, as opposed to the frequency of motion encoding, ω_g, during MRE. In the presence of motion encoding magnetic field gradients, G, which are used to store the magnitude of spin displacement along a given direction, the spins accumulate phase, ϕ, which is given by the expression (Eq. 2.3):

$$\phi = \gamma \int G\left(t\right)\cdot u_0 cos\left(\mathbf{k}\cdot\mathbf{r} + \omega_v t\right) dt, \tag{2.3}$$

where γ is the gyromagnetic ratio, and τ is the period of the encoding gradients given by $\tau = \frac{2\pi}{\omega_g}$. The typical MRE experiment uses a train of bipolar gradients that flip polarity with a specified frequency, ω_g. We will consider periodic gradients with trapezoidal lobes, which can be simplified to rectangular lobes with a constant amplitude G. With this representation of the bipolar gradients, the accumulated phase (for a single point in space) can be expressed as follows (Eq. 2.4):

$$\phi = \frac{\gamma\cdot G\cdot u_0\cdot\tau}{\pi\Omega} sin\left(\theta - \pi\Omega\right)\left[1 - cos\left(\pi\Omega\right)\right], \Omega = \frac{\omega_v}{\omega_g}, \tag{2.4}$$

where Ω is the ratio between the spin vibration and MRE encoding frequencies. When the motion encoding is synchronized with the vibration, the two frequencies are equal ($\Omega = 1$), and Eq. 2.4 takes a familiar form reported previously [1]. On the other hand, an encoding frequency that differs from the vibration frequency may be utilized to increase phase contrast [41], to shorten gradient length [14], or to encode multiple frequencies [56]. To capture wave propagation in time, the controlled phase offset θ is typically varied in even intervals across one period of vibration, or during a certain period, in order to obtain the desired spectral resolution when decomposing the encoded signal. However, if the vibration frequency is unknown, or if it differs from the expected frequency, there is no guarantee that the phase offsets will no longer be properly spaced, and the expression for phase should be adjusted to reflect this uncertainty. The phase offsets imposed through the sequence will be denoted by θ_g, and the resulting phase offset relative to the vibration will be $\theta_v = \Omega\theta_g$. The expression for phase can now be written as follows (Eq. 2.5):

$$\phi = \frac{\gamma \cdot G \cdot u_0 \cdot \tau}{\pi\Omega} sin\left(\theta_g - \pi\Omega\right)\left[1 - cos\left(\pi\Omega\right)\right]. \tag{2.5}$$

The above expression for phase accumulation applied to the case of encoding a vibration characterized by the resulting frequency ω_v, with MRE encoding gradients at an encoding frequency ω_g, in general different than ω_v. The distinction made between the two frequencies is necessitated by the influence of the cerebrospinal fluid and neck muscles on the head motion, or dynamic mismatch between the shaker and vibration transmission. Although the mechanical actuator is vibrating the cranium at one frequency, the brain, in principle, can vibrate at another. Because the desired phase offsets are no longer assumed to match the actual offsets for the vibration pattern, when the signal is decomposed using the Fourier transform [3] there will be errors in the output which affect the wave inversion procedure used to obtain the mechanical properties of the sample.

2.3 Methods

In order to investigate the effects of encoding off-frequency, two types of experiments were performed. First, numerical simulations were performed for a variety of frequency ratios. Second experiments were performed on a phantom as well as a human brain in vivo. The results were then compared to gain insight into the phenomenon of frequency mismatch.

2.3.1 Numerical Simulations

Displacement fields were simulated for shear waves propagating in a single direction through an elastic material. The material was modeled as a linear, homogenous, and isotropic medium with a shear stiffness of 3 kPa. The input (actuation) was an oscillatory 1D motion of the boundary with an amplitude of 100 μm, but without attenuation caused by viscoelastic damping. Wave patterns corresponding to actuation frequencies of 40, 45, 50, 55, and 60 Hz were simulated and MRE-encoded with a frequency of 50 Hz. This resulted in simulated MRE data sets for values of Ω at 0.8, 0.9, 1.0, 1.1, and 1.2, respectively.

The simulated encodings were based on acquisition schemes synchronized with 50 Hz, a typical value for a brain MRE experiment. Phase offsets were acquired over a single period of vibration at 50 Hz, and the data was processed using the same frequency. The simulated wave images were temporally Fourier-transformed and processed using a local frequency estimation inversion algorithm to determine the stiffness of the material.

2.3.2 Phantom and Brain Experiments

Experiments were performed with a closed, cylindrical agar gel phantom composed of a softer (2% agar) annulus surrounding a stiffer (3% agar) center column. The phantom was placed so that the cylindrical axis was in the anterior-posterior direction, and the entire phantom was vibrated in a rocking motion in the same direction using a homemade actuation system. A cradle that pivots along a structure attached to the head coil and a remote shaker made up the MRE actuation hardware system. The system was also used for the in vivo brain experiments on a single volunteer. The subject lies supine with the head resting on the cradle, which results in actuation in a nodding motion of the head.

A single-shot spin-echo echo-planar imaging (EPI) sequence, modified to include bipolar motion encoding gradients, was used in all experiments. Coronal images were acquired for the phantom, which provided a cross-sectional slice of the cylinder, and axial images were taken for the brain. All experiments were conducted using an encoding frequency of 50 Hz and forty phase offsets, while was performed at the same set of frequencies described in the numerical simulations section, above. Encoding was performed on a single axis (through-plane), with a motion encoding gradient amplitude of 30 mT/m. Other important imaging parameters included: FOV = 192 mm (240 mm for brain); matrix size = 64×64; TR/TE = 1000/90 ms; slice thickness = 5 mm. All experiments were performed on a Siemens 3T Allegra head-only scanner (Siemens Medical Systems, Erlangen, Germany) at the Beckman Institute of the University of Illinois at Urbana-Champaign.

The acquired phase data was subtracted, unwrapped, and spatially filtered using a Butterworth

bandpass filter to remove effects of bulk motion and noise. Finally, Fourier-transformed wave patterns were used as inputs to the same inversion algorithm described in the previous section.

2.4 Results

Figure 2.1 presents the apparent measured amplitude of the each simulated wave pattern in space, corresponding to the frequency ratios (Ω) described previously. The amplitude presented here is the magnitude of the complex signal at the first harmonic, as obtained from the temporal Fourier transform. Figure 2.2 shows the apparent elastic stiffness of the simulated material as would be measured with MRE for the different frequency ratios. For the frequency ratios that differ from the matched case ($\Omega = 1.0$), differences can be seen in the mean estimated stiffness across the material, as well as in local fluctuations within the sample. The variations in shear stiffness for the different frequency ratios relative to the matched case are summarized in Table 2.1. The total energy fractions of the harmonic spectra from the simulations are shown in Figure 2.3, with the inset depicting a detail of the first harmonic.

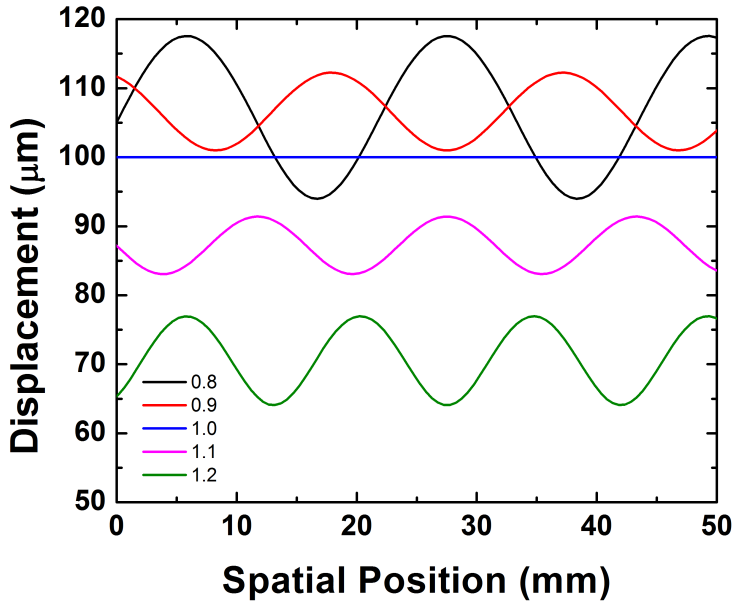

Figure 2.1: Results of the numerical solutions for different frequency ratios (Ω): 0.8, 0.9, 1.0, 1.1, and 1.2. Measured amplitude of the first harmonic versus spatial position.

The results of the phantom experiments are summarized in Figure 2.4. Wave images reconstructed from the first harmonic are presented along with the reconstructed stiffness maps for two "unmatched" frequency ratios, 0.8 and 1.2, for comparison with the matched frequency ratio, $\Omega = 1.0$. The results for

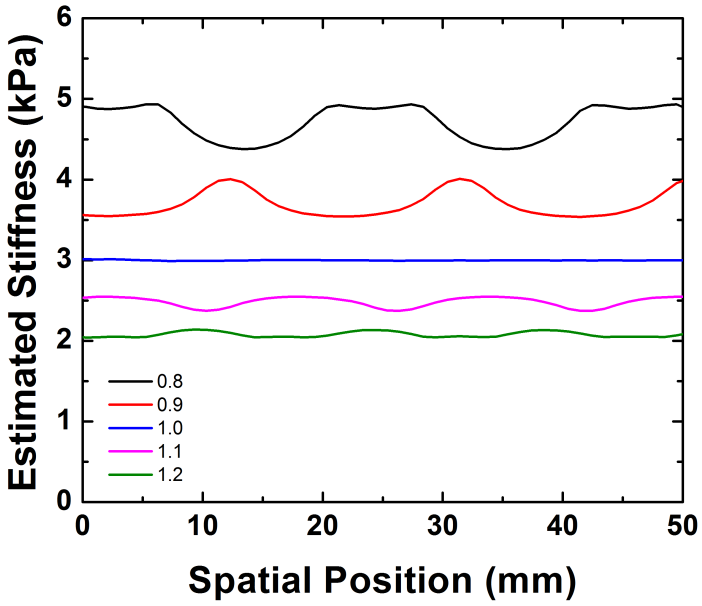

Figure 2.2: Results of the numerical solutions for different frequency ratios (Ω): 0.8, 0.9, 1.0, 1.1, and 1.2. Estimated stiffness versus spatial position.

brain experiments are presented in Figure 2.5, in the same format.

2.5 Discussion

MRE has been used to determine the stiffness of biological tissues in vivo and non-invasively, including the human brain. However, MRE methodology depends strictly on the knowledge of the driving frequency of mechanical actuation, and invalid assumptions regarding the dynamic system can lead to errors in acquisition parameters. In this work we have looked at how encoding at the incorrect frequency can manifest itself as artifacts in the computed stiffness map of the measured tissue.

It was shown through numerical simulations that encoding at a frequency other than that of either the actuator or vibrations resulting from actuation can lead to incorrect determination of the amplitude of vibration at the specific frequency of interest. As discussed previously, the acquisition of wave images in time is tailored specifically to the encoding frequency, and if the driving frequency is not strictly matched, a different portion of the vibration period will be acquired. When the data is decomposed into a Fourier series, the amplitude of the first harmonic will vary with spatial position, as demonstrated in Figure 2.1.

Variations of the signal amplitude in space directly influence the stiffness estimates at the same points in space. MRE inversion algorithms utilize the elastic wave equation to determine the stiffness from

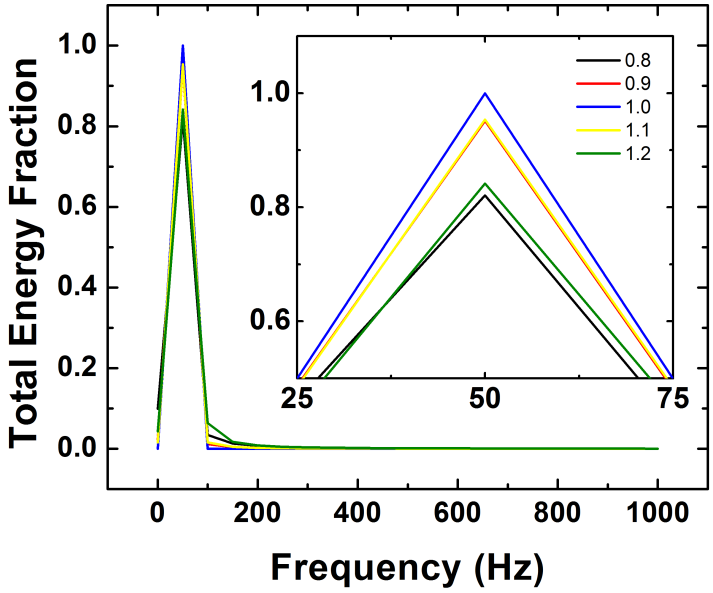

Figure 2.3: Results of the numerical solutions for different frequency ratios (Ω): 0.8, 0.9, 1.0, 1.1, and 1.2. Spectra of captured energy fraction, with detail of harmonic of interest (inset).

Table 2.1: Summary of estimated stiffness results of simulations at different frequency ratios: percent difference in mean stiffness compared to matched case, and percent maximum variation compared to mean stiffness with the sample

Frequency Ratio	**0.8**	**0.9**	**1.0**	**1.1**	**1.2**
Difference in Mean Stiffness(%)	56.7	24.1	0.00	17.6	30.6
Max. Variation from Mean Stiffness(%)	6.88	7.67	0.00	4.16	2.66

acquired displacement fields, and thus require the estimation of second derivates of the displacement in space. Local variations in wave amplitude are translated to locally stiffer or softer tissue; therefore, variations stemming from experimental errors will lead to the appearance of spurious stiffness variations in the medium, as demonstrated in Figure 2.2. Local variations up to 7.67% relative to the mean measured stiffness were found. In general, the variations were elevated for frequency ratios less than 1.0, and were the highest for the cases nearest matched frequencies. These results are summarized in Table 2.1.

Decomposition of the signal using the Fourier transform can reduce noise and is intended to isolate vibrations only at the frequency of interest, or the first Fourier harmonic. The total energy fractions for the different simulations are presented to demonstrate how small variations from the expected frequency are handled by the Fourier transform decomposition. Since the Fourier transform is a parametric technique with spectral results defined by acquisition parameters, leakage of the response at frequencies other than one specifically sampled for will be spread to other harmonics. It can be seen in Figure 2.3 that for all the

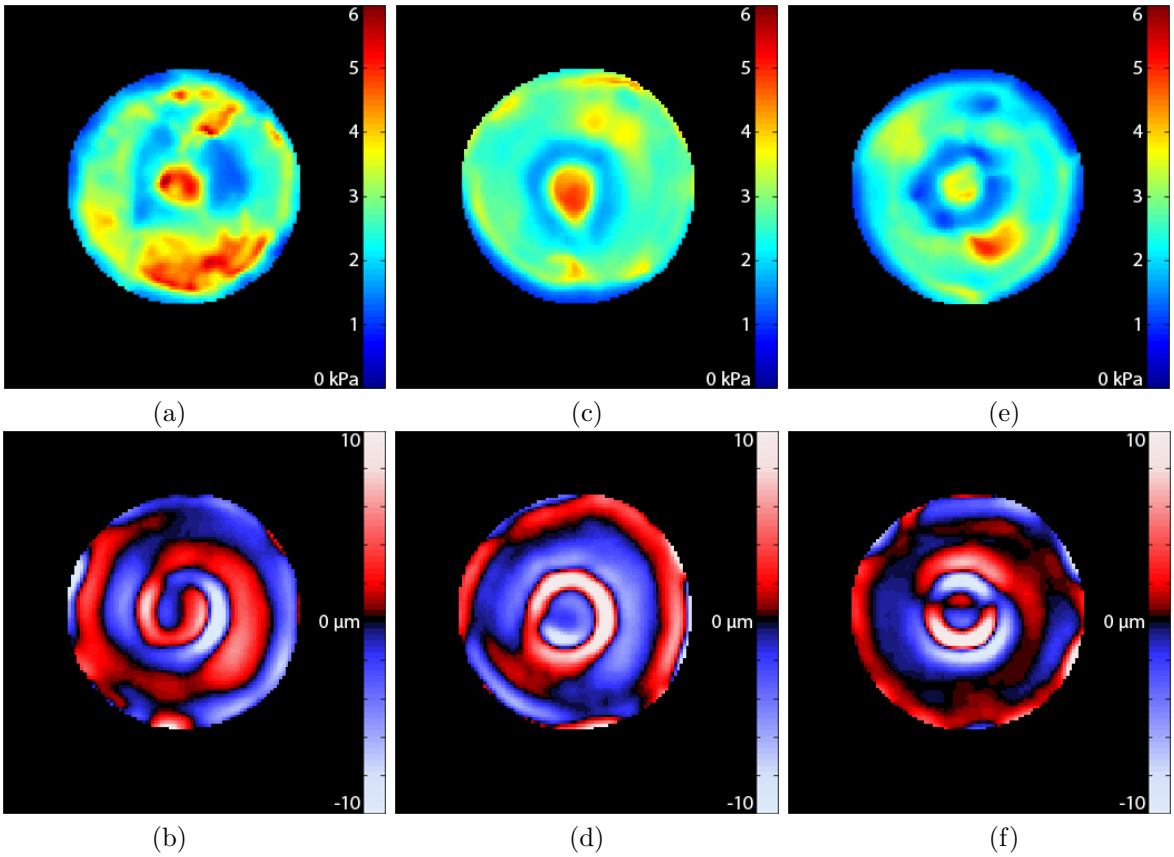

Figure 2.4: Stiffness maps for phantom experiment (top row) and corresponding mode shapes (bottom row) for frequency ratios: 0.8 V (a,b); 1.0 V (c,d); and 1.2 V (e,f).

simulations, with small variations in frequency, the first harmonic still carries a significant majority of the signal energy, and these variations are likely undetectable given signal-to-noise ratios in MRE experiments.

Knowledge of the driving frequency is essential for acquisition design, but is also important in the inversion process, as the inversion of the elastic wave equation involves multiplying measured magnitudes by the known frequency. When the entire MRE experiment is conducted with the "wrong" frequency, the calculated stiffness maps will be multiplied by the incorrect scalar value resulting in global inaccuracies. The estimated stiffness values presented in Figure 2.2 show mean values for the material stiffness that differ from the matched frequency case. Mean stiffness values were found to differ from the value of the sample by 56.7% for the ratio of 0.8 and 30.6% for the ratio of 1.2, and will be greatest for ratios furthest from 1.0. In addition to those regarding the stiffness variations in space, the results for mean stiffness are collected in Table 2.1.

The results of the phantom experiment demonstrate the consequences of performing an actual MRE experiment while encoding at the wrong frequency. When the frequencies are matched, the estimated stiffness of the material is as expected and the stiff center core is clearly distinguishable from the softer gel

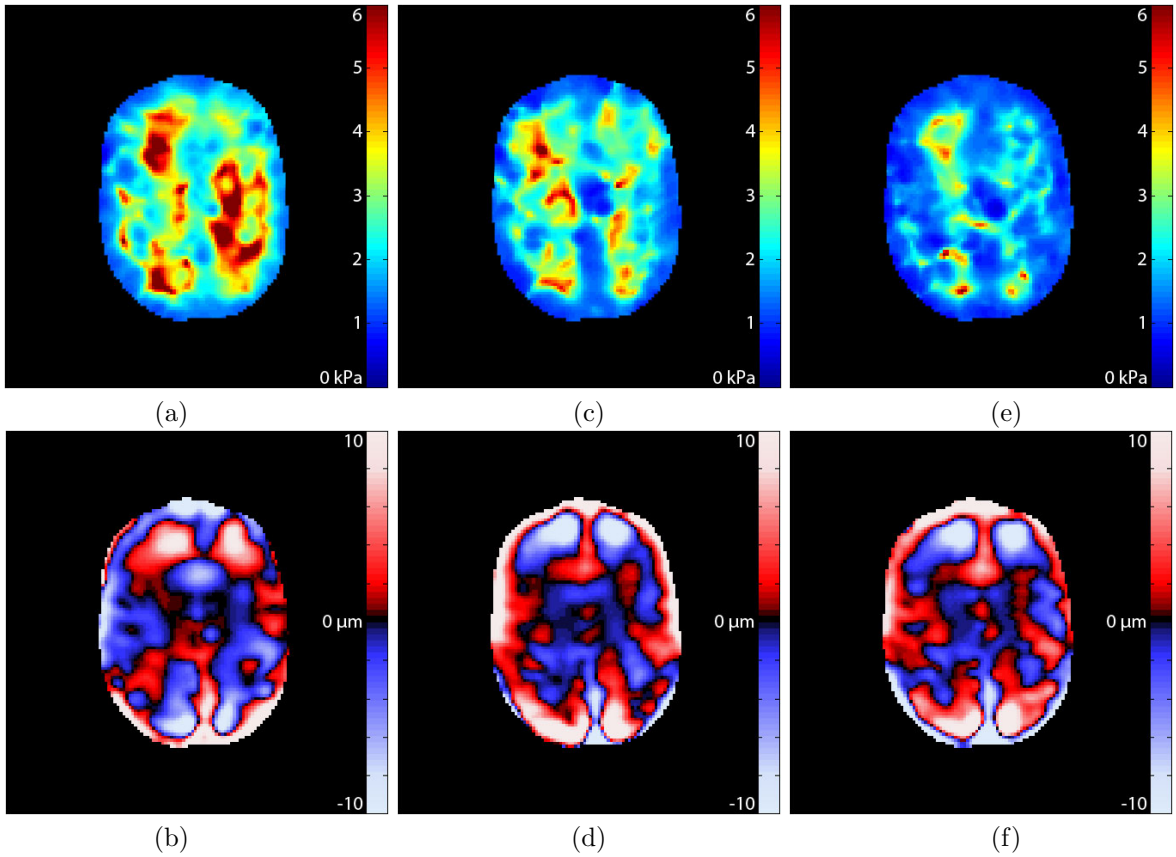

Figure 2.5: Stiffness maps for brain experiment (top row) and corresponding mode shapes (bottom row) for frequency ratios: 0.8 V (a,b); 1.0 V (c,d); and 1.2 V (e,f).

surrounding it. Consistent with the simulations, the global stiffness estimate for the experiment with the smaller frequency ratio is greater than the matched case, and for the larger ratio, the gel is estimated to be softer. It can also be noted that the variations of stiffness in space demonstrated in the simulation are present in the annulus for the off-frequency experiments, while the matched experiment shows the actual uniform distribution.

The wave patterns of the first harmonic are used in the inversion process to estimate the stiffness of the material. The acquired patterns for both the phantom and brain experiments are presented here to demonstrate that for the different frequency ratios there is no qualitative difference in measured displacements between the cases, other than what could be described as an arbitrary phase shift in the vibration period.

Experiments conducted on the human brain showed the same trends in global shear stiffness with changing frequency ratio as the phantom experiments. With the brain however, it becomes more difficult to distinguish the stiff structures that are in the brain from those that appear in the stiffness estimate due to off-frequency encoding. The stiffness maps estimated from experiments with all frequency ratios are not

qualitatively different from published results in this area, making it difficult to discern which is the truest representation of stiffness [16, 17, 18]. This further demonstrates that based on wave patterns and stiffness maps alone, there is not enough information to determine if the experiment has been conducted accurately.

2.6 Conclusions

In this section, we have demonstrated how synchronizing an MRE experiment to the incorrect mechanical frequency can lead to errors in the estimated stiffness of the imaged tissue. Off-frequency encoding, which can be caused by nonlinearities in the tissue or actuation system, can distort the estimates of both global and local shear stiffness. For the human brain, where dynamic nonlinearities are most likely, it was shown that an MRE experiment at the wrong frequency might produce results that are ambiguous or unreliable. Based on these findings, it is recommended that future MRE methods and studies account for the possibility of the presence of mismatched frequencies.

Chapter 3

Proper Orthogonal Decomposition for Improved Assessment of Brain MR Elastography

3.1 Introduction

One of the major issues surrounding MRE of the brain in recent studies has been its relative inability to provide reproducible results [16]. Depending on the specifics of the MRE methodologies used in brain experiments, in vivo results generally do not agree across clinical sites and studies [16, 17, 18]. The prevailing reason for this is that there are many MRE techniques that have been developed over the history of the method, and some provide better results than others. However, the complexity of the brain and its dynamic system may be the result of these discrepancies, not simply methods alone. MRE techniques rely on controlling the input displacement, and tailoring the experiment to match [3]. In a linear system, this is a straightforward task that should be relatively independent of experimental design. On the other hand, in a nonlinear system, which the brain ostensibly is [57, 58, 59], the dynamic response of the tissue to stimuli could be highly sensitive to minor changes in test parameters. These nonlinearities can occur both within the cranium as force is transmitted to the tissue and in the external mechanical actuation system, and can have a significant impact on MRE findings.

Typical MRE methodologies sample wave propagation in time, and use a Fourier transform (FT) to extract the displacements at the driving frequency of interest. In nonlinear systems, the FT is inadequate for decomposing the signal as it makes certain assumptions that cannot be guaranteed in a nonlinear system. Instead, a non-parametric technique called the proper orthogonal decomposition (POD) [60, 61, 62] is proposed in order to probe the dynamics of the nonlinear system with MRE. When investigating a nonlinear system, it is most useful to extract invariant manifolds or modes that are a low-order definition of the system dynamics, which can be the basis for larger dynamic models to be constructed. POD can be used to find these modes of the system by identifying those that carry the most vibrational energy through autocorrelation in both space and time [60, 63]. In contrast, FT modes are determined based only on the signal profile in time, and are largely dependent on the signal sampling

procedure. Achieving accurate and reproducible results through MRE for a nonlinear system using standard FT techniques could require a very large number of experiments to be performed, each with a different tailored acquisition scheme. However, finding the intrinsic response of the system could be obtainable through MRE with a single experiment if POD is used, which could lead to a fast, accurate, and repeatable estimate of the tissue properties.

In this work we investigated the nonlinearity of dynamic systems in MRE through both FT and POD methods. Phantom experiments were performed to provide a linear contrast to the ostensibly nonlinear brain system. The performance of the POD was also explored and quantified relative to the FT method to determine the optimal method for decomposing brain MRE data.

3.2 Theory

POD, also know as Karhunen-Loève decomposition, is a procedure for extracting a set of basis functions for modal decomposition from a series of signals in time and space [60]. POD has traditionally been applied in many fields of engineering including fluid dynamics [64], structural mechanics [65], and recently, medical imaging [66]. It is primarily used for model reduction in order to describe infinite-dimensional complex systems through a low-dimensional series of bases in order to probe the underlying dynamics of the system. In contrast to traditional modal analysis techniques, such as FT methods, POD is non-parametric and is not affected by nonlinearities or by closely spaced modes. To this end, POD has been shown to be the optimal decomposition technique in terms of capturing the most energy in the signal through the least number of extracted modes [60].

POD methods work by describing a temporally and spatially varying field using time-invariant spatial bases multiplied by spatially invariant temporal coefficients. In terms of its use in image processing, a time series of images denoted by ϕ can be decomposed according to Eq. 3.1:

$$\phi\left(x_i, y_j, t_n\right) = \sum_{k}^{K} \xi_k\left(x_i, y_j\right) a_k\left(t_n\right). \tag{3.1}$$

The spatial bases are denoted by ξ, and the temporal coefficients are denoted by a. The POD returns a number of bases and corresponding time series equal to the number of time points in the original series, N. Since it is the main use of POD lies in model order reduction, the number of included bases, K, is often less than N, thus providing a truncated approximation of the signal.

In a practical sense, POD modes are the eigenfunctions of the autocorrelation matrix, A, of the image field. The matrix A of a series of MxM images is constructed by organizing the spatial data into columns

for each time point, resulting in a M^2xN matrix A. The spatial bases are then determined by solving the eigenvalue problem (Eq. 3.2):

$$A^T A\xi = \eta\xi, \tag{3.2}$$

where η is the eigenvalue, or energy, associated with each mode. The time coefficients for each mode are further determined by projecting the base on to the original image series (Eq. 3.3):

$$a_k(t_n) = \sum_i^M \sum_j^M \xi_k(x_i, y_j)\, \phi_k(x_i, y_j, t_n). \tag{3.3}$$

The POD mode shapes are further used as the basis for investigating the true dynamics of the system through Galerkin projection methods seeking to solve the governing differential equation associated with the physical phenomenon [60, 67, 68, 69, 70].

3.3 Methods

To demonstrate how POD methods perform with MRE data, comparisons between POD and typical Fourier decompositions were made for both phantom and in vivo brain experiments.

3.3.1 Phantom and Brain Experiments

MRE experiments were performed with a homemade actuation system that comprises a remote shaker and rocker apparatus. The rocker was attached to the inside of the head coil and was connected to the shaker by means of a long rod [17], and the same system was used for both phantom and in vivo brain experiments. A closed, cylindrical agar gel phantom was used, which was composed of a softer (2% agar) annulus surrounding a stiffer (3% agar) center column. All experiments were performed on a Siemens 3T Allegra head-only scanner (Siemens Medical Systems, Erlangen, Germany) at the Beckman Institute of the University of Illinois at Urbana-Champaign.

Both the phantom and brain were actuated at a frequency of 50 Hz, with a range of input amplitudes corresponding to voltage levels from a function generator in LabVIEW (National Instruments, Austin, Texas). Separate experiments were performed using inputs of 1.5 V, 2.0 V, and 2.5 V, while all other experimental parameters were held constant.

A single-shot spin-echo echo-planar imaging (EPI) sequence, modified to include bipolar motion encoding gradients, was used in all experiments. Motion was encoded at 50 Hz with forty equally spaced

phase offsets over a single period of vibration. Encoding was performed on a single axis (thru-plane), with a motion encoding gradient amplitude of 30 mT/m. Imaging parameters included: FOV = 192 mm (240 mm for brain); matrix size = 64x64; TR/TE = 1000/90 ms; slice thickness = 5 mm. Acquired phase data was subtracted, unwrapped, and spatially filtered using a Butterworth bandpass filter to remove effects of bulk motion and noise.

3.3.2 Signal Decomposition

All data sets were decomposed in time using the Fourier transform, as is standard in MRE processing. Fourier mode shapes were obtained from the real and imaginary parts of the signal at the first harmonic for each voxel. The first harmonic corresponds to the driving frequency of the experiment, and if the system is linear, the mode shapes will be invariant with amplitude.

Data sets were also decomposed using the POD method. POD mode shapes were constructed in a similar fashion to the Fourier modes, by combining the first and second POD bases, which are the two highest energy-carrying bases returned by the decomposition. The two POD bases roughly correlate to the real and imaginary Fourier bases, as the found modes are complex. If the measured MRE response is an intrinsic property of the system, the POD modes should be invariant with amplitude, regardless of linearity.

To better quantify the performance of the two decomposition methods in capturing the vibrational response of the system, the energies of the modes were compared. The energy of the Fourier modes is defined by the square of the amplitude of the response at the first harmonic, summed over the image. The energies of the POD modes are the corresponding eigenvalues associated with the eigenvectors, or bases. Energy fractions are determined by dividing the energy of the mode of interest by the total energy in the system.

3.4 Results

The results of the phantom experiments are shown in Figure 3.1. The top row shows the Fourier mode shapes of the phantom acquired with MRE. These mode shapes are compared to the POD mode shapes extracted from the same data sets on the bottom row. The actuation intensities corresponding to the mode shapes are shown in decreasing order from left to right. The results from the brain experiments are presented in the same format in Figure 3.2.

Results of the energy fraction comparison for the phantom are presented in Figure 3.3. The fractional energy is plotted against the combination of the most energy-rich bases captured. The captured energy is

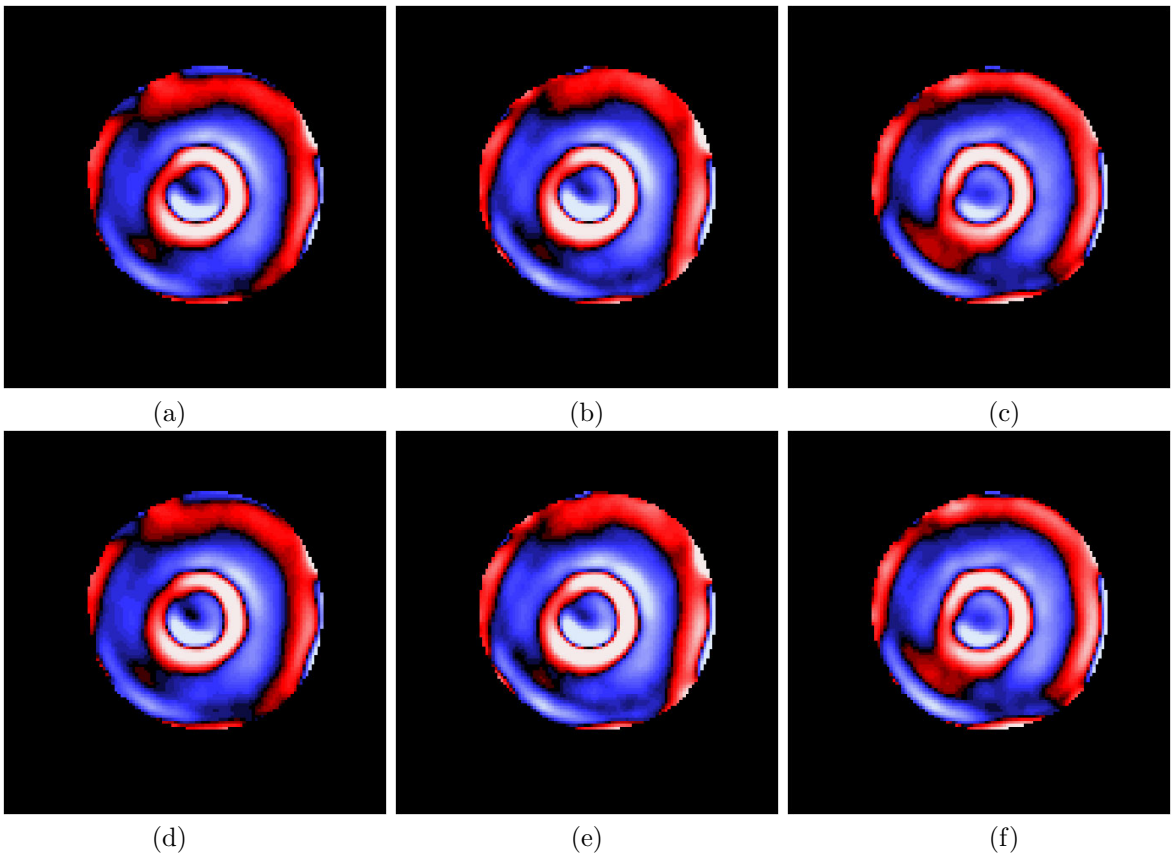

Figure 3.1: Mode shapes for the phantom experiment obtained with both FT (top row) and POD (bottom row) for actuation intensities: 2.5 V (a,d); 2.0 V (b,e); and 1.5 V (c,f).

compared for both Fourier and POD modes across all actuation intensities. The same comparison is performed for the brain experiments, and the results are presented in Figure 3.4. To compare the modes of interest, the energy fractions of the two most energy-rich bases were compared. For the phantom, the Fourier mode energy fraction, averaged across all actuation intensities, was found to be $84.7 \pm 1.5\%$, while the POD modes carried an energy fraction of $87.4 \pm 1.0\%$. For the brain modes, the Fourier modes had an energy fraction of $59.3 \pm 3.4\%$, while the POD returned an energy fraction of $73.7 \pm 1.9\%$. These results are summarized in Table 3.1.

Table 3.1: Summary of energy fractions carried by the FT and POD modes

	Phantom	**Brain**
FT Mode Energy Fraction (%)	84.7 ± 1.5	59.3 ± 3.4
POD Mode Energy Fraction (%)	87.4 ± 1.0	73.7 ± 1.9

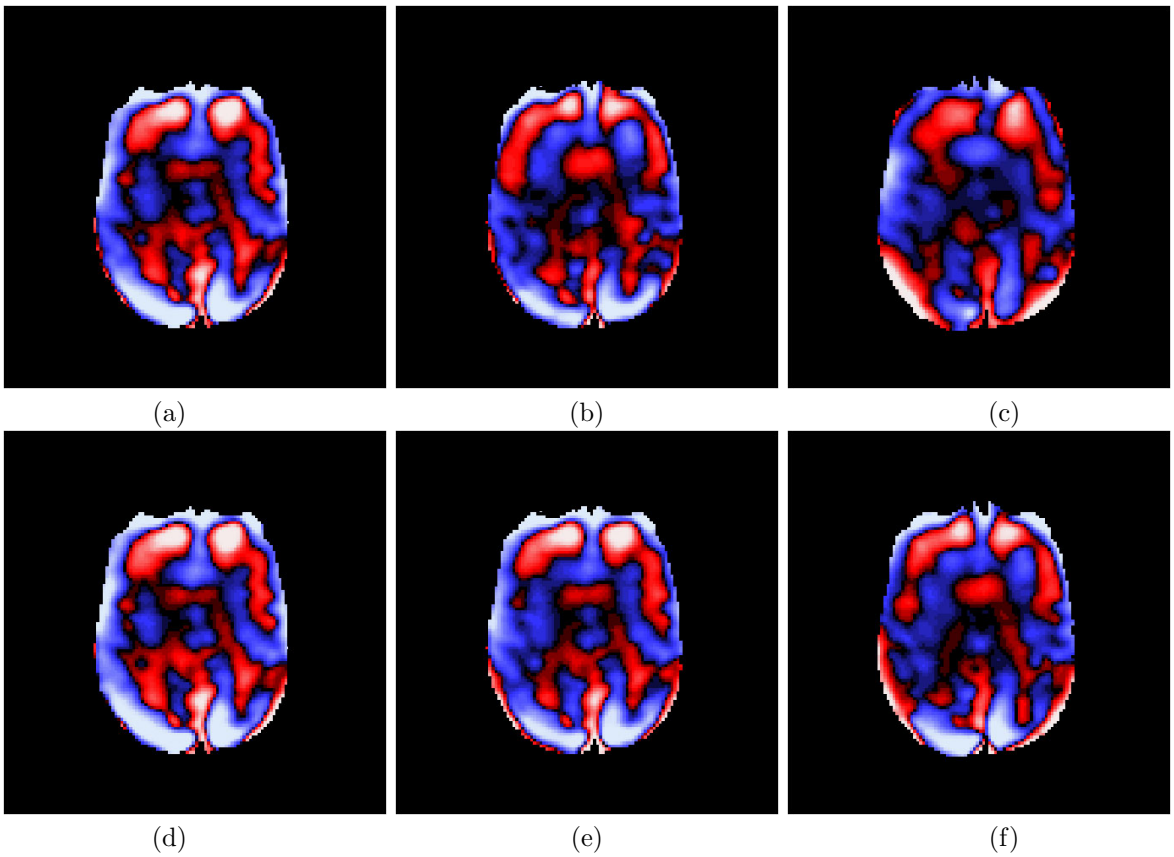

Figure 3.2: Mode shapes for the brain experiment obtained with both FT (top row) and POD (bottom row) for actuation intensities: 2.5 V (a,d); 2.0 V (b,e); and 1.5 V (c,f).

3.5 Discussion

One of the fundamental assumptions of MRE is that the dynamic system is linear. This assumption implies that the intrinsic response of the system is invariant, and that displacement patterns will only scale with amplitude. If nonlinearities are introduced in the dynamic system, the response will depend on actuation amplitude, and the results obtained with MRE with a given actuation would not be the same as with another. In this work, we have used POD to investigate nonlinearity in MRE, and sought to quantify the performance of the method.

The results from the phantom experiment were used to compare FT and POD mode shapes. Based on visual inspection of Figure 3.1, it can be seen that, based on visual inspection, the FT mode shapes are very similar across all actuation intensities. Small changes in overall shape can possibly be attributed to relative contrast-to-noise ratio changes with amplitude. The same observations can be made when comparing the POD modes across intensity. More importantly, the FT and POD mode shapes agree at each level of actuation intensity. Since the FT modes would only be invariant and correlate with the POD

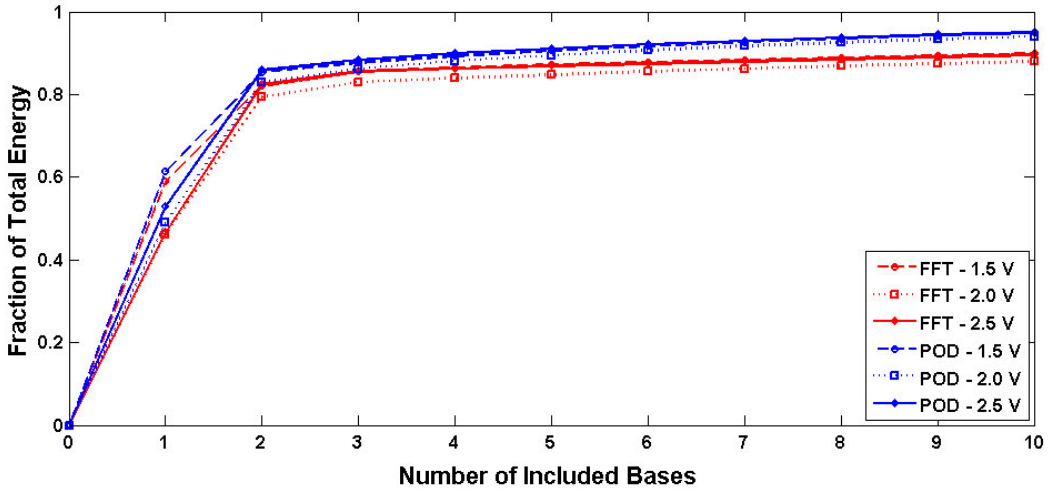

Figure 3.3: Captured energy fractions for modes obtained with both FT and POD in the phantom for all actuation intensities vs. number of included bases.

modes in the case of dynamic linearity, the results confirm that the phantom system is linear, as expected.

Comparing the captured energy profiles from both decomposition methods further confirms the phantom results. As seen in Figure 3.3, the captured energy fractions are very similar for both methods, with POD performing slightly better. It can also be observed that the energy fractions are nearly the same for both methods for all intensity levels. When looking at a single mode of interest, both methods capture a very large fraction of energy, with POD capturing more energy and with only a small variation with intensity. The observation of linearity is further confirmed in this case, and POD is shown to be a better method of decomposition of MRE results.

Upon examination of the results of the brain experiments, it is evident that the FT mode shapes, shown in Figure 3.2, are not invariant as actuation intensity changes. With decreasing intensity, the modes change shape, and they no longer correlate with the POD mode shapes. However, the POD shapes are seemingly invariant with actuation intensity, similar to the phantom experiment. Based on this observation, it appears that the dynamic brain system is nonlinear, as expected, and that the POD modes may represent an intrinsic response of the system.

The captured energy fractions are compared for the two methods across actuation intensities to provide a quantification of the brain results. In Figure 3.4 it is clearly demonstrated that POD modes carry significantly more energy than the corresponding FT modes. It is also notable that for the mode of interest, neither method captured the same energy fraction across intensity, but the POD modes had much less variation. This further suggests that the POD mode may be intrinsic to the system, and again confirms the performance of POD over Fourier decomposition.

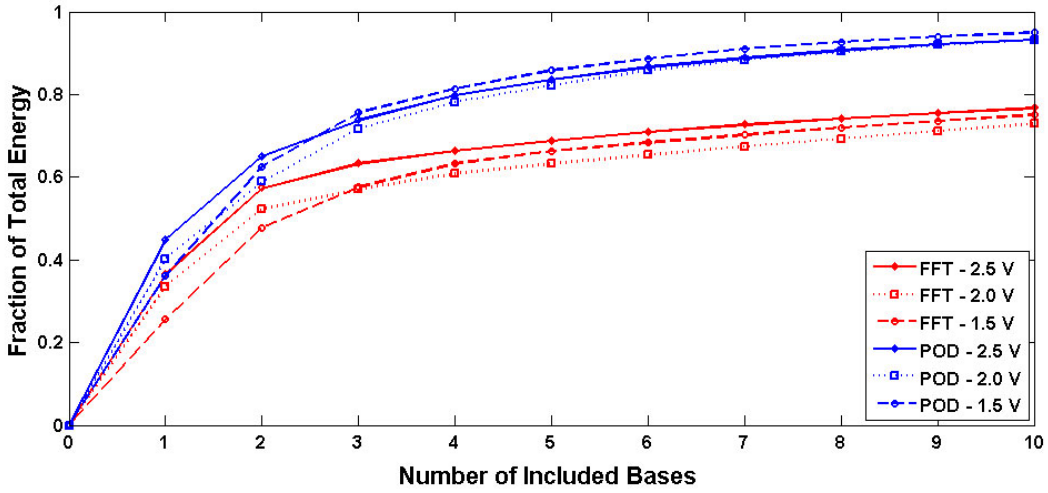

Figure 3.4: Captured energy fractions for modes obtained with both FT and POD in the brain for all actuation intensities vs. number of included bases.

3.6 Conclusions

This section addressed the performance of MRE techniques in the presence of nonlinearities in the dynamic system of interest. MRE experiments on a nonlinear dynamic system may result in errors in the stiffness results due to the amplitude dependent response of the system, and results may be irreproducible with different conditions. We have shown through comparison of Fourier and POD modes that the human brain as a dynamic system demonstrates nonlinear behavior, as compared to experiments on a phantom. POD was shown to optimally capture the vibrational energy in MRE experiments, and the POD modes appear to provide information about the intrinsic properties of the system and its response to mechanical actuation. These POD modes may then be used as the basis for a Galerkin projection, or other computational technique, to generate a low-dimensional model of the dynamic brain system, and provide a more accurate assessment of the mechanical properties of brain tissue with MRE.

Chapter 4

Summary and Conclusions

The scope of this thesis was the investigation of the effect of nonlinearity of the system on magnetic resonance elastography. Brain elastography can provide quantitative estimates of the shear modulus of brain tissue in vivo, and in that sense it is extremely useful to both clinicians and researchers alike. Despite the success MRE methods have enjoyed in investigating tissues such as liver and breast, care must be taken to ensure that accurate results are being obtained when applying the methods to more complex tissues, like the brain. The inherent nonlinearity of the brain dynamic system can introduce MRE artifacts. In this work, we focused on the effects of uncertainties in actuation frequency and amplitude.

The presence of vibrations at unknown or undesired frequencies was shown to have a significant effect on estimates of shear stiffness obtained with MRE on both local and global scales. Experiments driven with frequency difference from the encoding frequency were shown to result in spurious local spatial variations in shear stiffness, and to misrepresent global stiffness across the tissue. In brain MRE studies investigating lesions or diffuse diseases, these erroneous results can give false positives or false negatives.

The proper orthogonal decomposition method was implemented to further study the nonlinear behavior of the dynamic brain system, and was shown to elucidate the nonlinear effects in the response of the system to different amplitudes of forcing. The dependence of POD modes across actuation levels was studied to demonstrate that they could indeed represent intrinsic modes of system response because they remain invariant with amplitude of actuation. Our results indicate that POD is a better method of signal decomposition than standard Fourier techniques, and could lead to more accurate and reproducible estimates of the mechanical properties of brain tissue.

Investigating nonlinear effects with MRE is not new, but most of the work done has focused on nonlinearity of the tissue per se, and not on the overall dynamic system comprising actuator, cranium, and brain. It has been shown in this work that the overall nonlinear behavior can have a significant impact on MRE results and must be considered when investigating the brain. As methodologies grow and mature for brain MRE, the complexities of the tissue and actuation system must be accounted for through

modifications to acquisition schemes, mechanical actuation hardware, tissue deformation models, and property extraction methodologies. With POD, we propose a tool to understand the dynamic response of the overall system. Future work in this area will focus on system reduction by using the POD modes in a Galerkin projection to construct a low-dimensional model of the dynamics of the overall system. The inputs of the system are the MRE snapshots and not the detailed local dynamical models of the components, which are fraught with uncertainty. This model could lead to significant improvements in brain MRE, both in accuracy and reproducibility, and can be the next step in MRE methodology for the brain.

References

[1] Muthupillai, R., D. J. Lomas, P. J. Rossman, J. F. Greenleaf, A. Manduca, and R. L. Ehman (1995) "Magnetic Resonance Elastography by Direct Visualization of Propagating Acoustic Strain Waves," *Science*, **269**(5232), pp. 1854–1857.

[2] Plewes, D. B., I. Betty, S. N. Urchuk, and I. Soutar (1995) "Visualizing Tissue Compliance with MR Imaging," *J Magn Reson Im*, **5**(6), pp. 733–738.

[3] Manduca, A., T. E. Oliphant, M. A. Dresner, J. L. Mahowald, S. A. Kruse, E. Amromin, J. P. Felmlee, J. F. Greenleaf, and R. L. Ehman (2001) "Magnetic Resonance Elastography: Non-Invasive Mapping of Tissue Elasticity," *Med Image Anal*, **5**(4), pp. 237–254.

[4] Huwart, L., F. Peeters, R. Sinkus, L. Annet, N. Salameh, L. C. ter Beek, Y. Horsmans, and B. E. V. Beers (2006) "Liver Fibrosis: Non-Invasive Assessment with MR Elastography," *NMR Biomed*, **19**(2), pp. 173–179.

[5] Rouvière, O., M. Yin, M. A. Dresner, P. J. Rossman, L. J. Burgart, J. L. Fidler, and R. L. Ehman (2006) "MR Elastography of the Liver: Preliminary Results," *Radiology*, **240**(2), pp. 440–448.

[6] Klatt, D., P. Asbach, J. Rump, S. Papazoglou, R. Somasundaram, J. Modrow, J. Braun, and I. Sack (2006) "In Vivo Determination of Hepatic Stiffness Using Steady-State Free Precession Magnetic Resonance Elastography," *Invest Radiol*, **41**(12), pp. 841–848.

[7] Sinkus, R., J. Lorenzen, D. Schrader, M. Lorenzen, M. Dargatz, and D. Holz (2000) "High-Resolution Tensor MR Elastography for Breast Tumour Detection," *Phys Med Biol*, **45**(6), pp. 1649–1664.

[8] Plewes, D. B., J. Bishop, A. Samani, and J. Sciarretta (2000) "Visualization and Quantification of Breast Cancer Biomechanical Properties with Magnetic Resonance Elastography," *Phys Med Biol*, **45**(6), pp. 1591–1610.

[9] McKnight, A. L., J. L. Kugel, P. J. Rossman, A. Manduca, L. C. Hartmann, and R. L. Ehman (2002) "MR elastography of breast cancer: Preliminary results," *Am J Roentgenol*, **178**(6), pp. 1411–1417.

[10] Dresner, M. A., G. H. Rose, P. J. Rossman, R. Muthupillai, A. Manduca, and R. L. Ehman (2001) "Magnetic Resonance Elastography of Skeletal Muscle," *J Magn Reson Im*, **13**(2), pp. 269–276.

[11] Uffmann, K., S. Maderwald, W. Ajaj, C. Galban, S. Mateiescu, H. H. Quick, and M. E. Ladd (2004) "In Vivo Elasticity Measurements of Extremity Skeletal Muscle with MR Elastography," *NMR Biomed*, **17**(4), pp. 181–190.

[12] Papazoglou, S., J. Braun, U. Hamhaber, and I. Sack (2005) "Two-Dimensional Waveform Analysis in MR Elastography of Skeletal Muscles," *Phys Med Biol*, **50**(6), pp. 1313–1325.

[13] Bensamoun, S. F., S. I. Ringleb, L. Littrell, Q. Chen, M. D. Brennan, R. L. Ehman, and K.-N. An (2006) "Determination of Thigh Muscle Stiffness Using Magnetic Resonance Elastography," *J Magn Reson Im*, **23**(2), pp. 242–247.

[14] Sack, I., J. Rump, T. Elgeti, A. Samani, and J. Braun (2009) "MR Elastography of the Human Heart: Noninvasive Assessment of Myocardial Elasticity Changes by Shear Wave Amplitude Variations," *Magn Reson Med*, **61**(3), pp. 668–677.

[15] Robert, B., R. Sinkus, J.-L. Gennisson, and M. Fink (2009) "Application of DENSE-MR-Elastography to the Human Heart," *Magn Reson Med*, **62**(5), pp. 1155–1163.

[16] Kruse, S. A., G. H. Rose, K. J. Glaser, A. Manduca, J. P. Felmlee, C. R. Jack, and R. L. Ehman (2008) "Magnetic Resonance Elastography of the Brain," *NeuroImage*, **39**(1), pp. 231–237.

[17] Sack, I., B. Beierbach, U. Hamhaber, D. Klatt, and J. Braun (2008) "Non-Invasive Measurement of Brain Viscoelasticity Using Magnetic Resonance Elastography," *NMR Biomed*, **21**(3), pp. 265–271.

[18] Green, M. A., L. E. Bilston, and R. Sinkus (2008) "In Vivo Brain Viscoelastic Properties Measured by Magnetic Resonance Elastography," *NMR Biomed*, **21**(7), pp. 755–764.

[19] McCracken, P. J., A. Manduca, J. P. Felmlee, and R. L. Ehman (2005) "Mechanical transient-based magnetic resonance elastography," *Magn Reson Med*, **53**(3), pp. 628–639.

[20] Hamhaber, U., I. Sack, S. Papazoglou, J. Rump, D. Klatt, and J. Braun (2007) "Three-dimensional analysis of shear wave propagation observed by in vivo magnetic resonance elastography of the brain," *Acta Biomater*, **3**(1), pp. 127–137.

[21] Xu, L., Y. Lin, Z. N. Xi, H. Shen, and P. Y. Gao (2007) "Magnetic resonance elastography of the human brain: A preliminary study," *Acta Radiol*, **48**(1), pp. 112–115.

[22] Papazoglou, S., C. Xu, U. Hamhaber, E. Siebert, G. Bohner, R. Klingebiel, J. Braun, and I. Sack (2009) "Scatter-based magnetic resonance elastography," *Phys Med Biol*, **54**(7), pp. 2229–2241.

[23] Arbogast, K. B. and S. S. Margulies (1999) "A fiber-reinforced composite model of the viscoelastic behavior of the brainstem in shear," *J Biomech*, **32**(8), pp. 865–870.

[24] Miller, K. and K. Chinzei (2002) "Mechanical properties of brain tissue in tension," *J Biomech*, **35**(4), pp. 483–490.

[25] Hrapko, M., J. A. W. van Dommelen, G. W. M. Peters, and J. S. H. M. Wismans (2008) "Characterisation of the mechanical behaviour of brain tissue in compression and shear," *Biorheology*, **45**(6), pp. 663–676.

[26] Cheng, S., E. C. Clarke, and L. E. Bilston (2008), "Rheological properties of the tissues of the central nervous system: A review," .

[27] Ahmida, K. M. and J. R. F. Arruda (2002) "On the relation between complex modes and wave propagation phenomena," *J Sound Vib*, **255**(4), pp. 663–684.

[28] Vakakis, A. F. (2002) *Normal Modes and Localization in Nonlinear Systems*, Springer, New York.

[29] Nayfeh, A. H. and D. T. Mook (1985) *Nonlinear Oscillations*, John Wiley and Sons, New York.

[30] Guckenheimer, J. and P. Holmes (1983) *Nonlinear Oscillations, Dynamical Systems, and Bifurcations of Vector Fields*, Springer, New York.

[31] Uffmann, K. and M. E. Ladd (2008) "Actuation systems for MR elastography," *IEEE Eng Med Biol*, **27**(3), pp. 28–34.

[32] Tse, Z. T. H., H. Janssen, A. Hamed, M. Ristic, I. Young, and M. Lamperth (2009) "Magnetic resonance elastography hardware design: a survey," *P I Mech Eng H*, **223**(H4), pp. 497–514.

[33] Braun, K., J. Braun, and I. Sack (2003) "Electromagnetic actuator for generating variably oriented shear waves in MR elastography," *Magn Reson Med*, **50**(1), pp. 220–222.

[34] Mariappan, Y. K., P. J. Rossman, K. J. Glaser, A. Manduca, and R. L. Ehman (2009) "Magnetic Resonance Elastography with a Phased-array Acoustic Driver System," *Magn Reson Med*, **61**(3), pp. 678–685.

[35] Uffmann, K., C. Abicht, W. Grote, H. H. Quick, and M. E. Ladd (2002) "Design of an MR-Compatible piezoelectric actuator for MR elastography," *Concept Magnetic Res*, **15**(4), pp. 239–254.

[36] Yin, M., O. Rouvière, K. J. Glaser, and R. L. Ehman (2008) "Diffraction-biased shear wave fields generated with longitudinal magnetic resonance elastography drivers," *Magn Reson Imaging*, **26**(6), pp. 770–780.

[37] Wuerfel, J., F. Paul, B. Beierbach, U. Hamhaber, D. Klatt, S. Papazoglou, F. Zipp, P. Martus, J. Braun, and I. Sack (2010) "MR-elastography reveals degradation of tissue integrity in multiple sclerosis," *NeuroImage*, **49**(3), pp. 2520–2525.

[38] Wang, H., J. B. Weaver, M. M. Doyley, F. E. Kennedy, and K. D. Paulsen (2008) "Optimized motion estimation for MRE data with reduced motion encodes," *Phys Med Biol*, **53**(8), pp. 2181–2196.

[39] Manduca, A., D. S. Lake, S. A. Kruse, and R. L. Ehman (2003) "Spatio-temporal directional filtering for improved inversion of MR elastography images," *Med Image Anal*, **7**(4), pp. 465–473.

[40] Sinkus, R., M. Tanter, T. Xydeas, S. Catheline, J. Bercoff, and M. Fink (2005) "Viscoelastic shear properties of in vivo breast lesions measured by MR elastography," *Magn Reson Imaging*, **23**(2), pp. 159–165.

[41] Rump, J., D. Klatt, J. Braun, C. Warmuth, and I. Sack (2007) "Fractional Encoding of Harmonic Motions in MR Elastography," *Magn Reson Med*, **57**(2), pp. 388–395.

[42] Bieri, O., S. Maderwald, M. E. Ladd, and K. Scheffler (2006) "Balanced alternating steady-state elastography," *Magn Reson Med*, **55**(2), pp. 233–241.

[43] Glaser, K. J., J. P. Felmlee, and R. L. Ehman (2006) "Rapid MR elastography using selective excitations," *Magn Reson Med*, **55**(6), pp. 1381–1389.

[44] Bensamoun, S. F., K. J. Glaser, S. I. Ringleb, Q. Chen, R. L. Ehman, and K.-N. An (2008) "Rapid magnetic resonance elastography of muscle using one-dimensional projection," *J Magn Reson Im*, **27**(5), pp. 1083–1088.

[45] Maderwald, S., K. Uffmann, C. Galban, A. de Greiff, and M. E. Ladd (2006) "Accelerating MR elastography: A multiecho phase-contrast gradient-echo sequence," *J Magn Reson Im*, **23**(5), pp. 774–780.

[46] Oliphant, T. E., A. Manduca, R. L. Ehman, and J. F. Greenleaf (2001) "Complex-valued stiffness reconstruction for magnetic resonance elastography by algebraic inversion of the differential equation," *Magn Reson Med*, **45**(2), pp. 299–310.

[47] Sinkus, R., M. Tanter, S. Catheline, J. Lorenzen, C. Kuhl, E. Sondermann, and M. Fink (2005) "Imaging anisotropic and viscous properties of breast tissue by magnetic resonance-elastography," *Magn Reson Med*, **53**(2), pp. 372–387.

[48] Sack, I., B. Beierbach, J. Wuerfel, D. Klatt, U. Hamhaber, S. Papazoglou, P. Martus, and J. Braun (2009) "The impact of aging and gender on brain viscoelasticity," *NeuroImage*, **46**(3), pp. 652–657.

[49] Perrinez, P. R., F. E. Kennedy, E. E. W. V. Houten, J. B. Weaver, and K. D. Paulsen (2009) "Modeling of Soft Poroelastic Tissue in Time-Harmonic MR Elastography," *IEEE T Bio-Med Eng*, **56**(3), pp. 598–608.

[50] Braun, J., G. Buntkowsky, J. Bernarding, T. Tolxdorff, and I. Sack (2001) "Simulation and analysis of magnetic resonance elastography wave images using coupled harmonic oscillators and Gaussian local frequency estimation," *Magn Reson Imaging*, **19**(5), pp. 703–713.

[51] Sack, I., J. Bernarding, and J. Braun (2002) "Analysis of wave patterns in MR elastography of skeletal muscle using coupled harmonic oscillator simulations," *Magn Reson Imaging*, **20**(1), pp. 95–104.

[52] Papazoglou, S., U. Hamhaber, J. Braun, and I. Sack (2008) "Algebraic Helmholtz inversion in planar magnetic resonance elastography," *Phys Med Biol*, **53**(12), pp. 3147–3158.

[53] Grimm, R. C., D. S. Lake, A. Manduca, and R. L. Ehman (2006) MRE / Wave. Rochester (MN): Mayo Clinic. Available from http://mayoresearch.mayo.edu/mayo/research/ehman_lab.

[54] Sack, I., C. K. Macgowan, A. Samani, C. Luginbuhl, W. Oakden, and D. B. Plewes (2004) "Observation of Nonlinear Shear Wave Propagation Using Magnetic Resonance Elastography," *Magn Reson Med*, **52**(4), pp. 842–850.

[55] Plewes, D. B., C. Luginbuhl, C. K. Macgowan, and I. Sack (2004) "An Inductive Method to Measure Mechanical Excitation Spectra for MRI Elastography," *Concept Magn Reson B*, **21B**(1), pp. 32–39.

[56] Klatt, D., U. Hamhaber, P. Asbach, J. Braun, and I. Sack (2007) "Noninvasive Assessment of the Rheological Behavior of Human Organs Using Multifrequency MR Elastography: A Study of Brain and Liver Viscoelasticity," *Phys Med Biol*, **52**(24), pp. 7281–7294.

[57] Charalambopoulos, A., G. Dassios, D. I. Fotiadis, and C. V. Massalas (1998) "Dynamic characteristics of the human skull-brain system," *Math Comput Model*, **27**(2), pp. 81–101.

[58] Linninger, A. A., M. Xenos, B. Sweetman, S. Ponkshe, X. Guo, and R. Penn (2009) "A mathematical model of blood, cerebrospinal fluid and brain dynamics," *J Math Biol*, **59**(6), pp. 729–759.

[59] Charalambopoulos, A., D. I. Fotiadis, A. Ktena, and C. V. Massalas (1998) "The effect of viscoelastic brain on the dynamic characteristics of the human skull-brain system," *Acta Mech*, **130**(3-4), pp. 159–173.

[60] Holmes, P., J. L. Lumley, and G. Berkooz (1996) *Turbulence, Coherent Structures, Dynamical Systems, and Symmetry*, Cambridge University Press, Cambridge, New York.

[61] Kerschen, G., J. Golinval, A. F. Vakakis, and L. A. Bergman (2005) "The method of proper orthogonal decomposition for dynamical characterization and order reduction of mechanical systems: An overview," *Nonlinear Dynam*, **41**(1-3), pp. 147–169.

[62] Chatterjee, A. (2000) "An introduction to the proper orthogonal decomposition," *Curr Sci India*, **78**(7), pp. 808–817.

[63] Jolliffe, I. T. (2002) *Principal Component Analysis*, Springer, New York.

[64] Berkooz, G., P. Holmes, and J. L. Lumley (1993) "The Proper Orthogonal Decomposition in the Analysis of Turblent Flows," *Annu Rev Fluid Mech*, **25**, pp. 539–575.

[65] Feeny, B. and R. Kappagantu (1998) "On the physical interpretation of proper orthogonal modes in vibrations," *J Sound Vib*, **211**(4), pp. 607–616.

[66] Kolen, A. F., N. R. Miller, E. E. Ahmed, and J. C. Bamber (2004) "Characterization of cardiovascular liver motion for the eventual application of elasticity imaging to the liver in vivo," *Phys Med Biol*, **49**(18), pp. 4187–4206.

[67] Morton, K. W. (1985) "Generalized Galerkin Methods for Hyperbolic Problems," *Comput Method Appl M*, **52**(1-3), pp. 847–871.

[68] Gottlieb, D. and D. Xiu (2008) "Galerkin method for wave equations with uncertain coefficients," *Commun Comput Phys*, **3**(2), pp. 505–518.

[69] Kunisch, K. and S. Volkwein (2001) "Galerkin proper orthogonal decomposition methods for parabolic problems," *Numer Math*, **90**(1), pp. 117–148.

[70] Rapun, M.-L. and J. M. Vega (2010) "Reduced order models based on local POD plus Galerkin projection," *J Comput Phys*, **229**(8), pp. 3046–3063.